JOURNAL OF NANO AND MATERIALS SCIENCE RESEARCH
Volume 3, No. 3 (Special Issue, 2026), pp. 56 – 63
Available online at journals.nanotechunn.com/jnmsr

ORIGINAL ARTICLE

Effect of Complexing Agents on Cadmium Sulfide (CdS) Deposition for Buffer Layer Application in Solar Cells

Onyekachi Nwakanma[a,*]

[a]*Department of Physics and Astronomy, Faculty of Physical Sciences, University of Nigeria, Nsukka, Enugu State 410101, Nigeria*

KEYWORDS

Cadmium sulfide;
Chemical bath deposition;
Complexing agent;
Buffer layer;
Thin-film solar cells

ARTICLE HISTORY

Received: June 06, 2026
Revised: June 25, 2026
Accepted: July 02, 2026
Published: July 16, 2026

ABSTRACT

This study explored the use of acetylacetone as a supplementary co-complexing agent alongside ammonia, rather than as a sole or replacement complexing agent, deposited by chemical bath deposition (CBD), and systematically investigated and compared the effects of films deposited with acetylacetone against those deposited without it. X-ray diffraction (XRD) analysis confirmed the hexagonal wurtzite crystal structure of both samples, while scanning electron microscopy (SEM) revealed quasi-spherical nanoparticles with average grain sizes of 50 – 100 nm and a binary chemical composition, with no detectable impurity phases. In comparison, atomic force microscopy (AFM) revealed an anisotropic surface topography, with elongated ridge features confined to a peak-to-valley height of ~27 nm. The bandgap studies using Tauc plot analysis explored the optical bandgap values. The Hall effect measurements of the acetylacetone-modified film confirmed n-type conductivity with a free electron concentration of 4.02×10^{10} cm^{-3}, Hall mobility of 49.2 cm^2/V·s, and electrical resistivity of 3.78×10^6 Ω·cm, collectively indicating a high-quality, low-defect-density semiconductor. The results demonstrate that acetylacetone serves as an effective co-complexing agent, markedly improving the optoelectronic properties of CBD-CdS films for buffer-layer integration in heterojunction solar cells.

1 Introduction

Thin-film photovoltaic technologies have attracted sustained global research interest as low-cost alternatives to conventional crystalline silicon solar cells, owing to their reduced material consumption, compatibility with large-area fabrication, and competitive power conversion efficiencies.

Among these, chalcopyrite-based Cu(In,Ga)Se_2 (CIGS) and cadmium telluride (CdTe) devices have achieved certified efficiencies exceeding 23% and 22%, respectively, firmly establishing them at the frontier of thin-film photovoltaics [1].

The continued advancement of these technologies depends critically on optimizing each functional layer, particularly the n-type buffer layer, which forms the heterojunction interface with the p-type absorber and governs charge transport, interface recombination, and the collection of photogenerated carriers.

Cadmium sulfide (CdS) remains the most widely adopted buffer material in high-efficiency thin-film solar cells, owing to its favorable band alignment with CIGS and CdTe absorbers, wide direct bandgap of approximately 2.42 eV, high optical transmittance in the visible range, and excellent surface passivation capability [2].

The state-of-the-art CdS buffer layer, deposited by chemical bath deposition (CBD), has been used successfully for several years, and its deployment has helped push device efficiencies above 20% [3]–[7]. The complexing agent plays a decisive role in CBD by coordinating with Cd^{2+} ions to regulate free ion activity, control supersaturation, and suppress bulk

* **CORRESPONDING AUTHOR** | O. Nwakanma, ✉ onyekachi.nwakanma@unn.edu.ng

precipitation so that, without any complexing agent, little to no film formation is anticipated on the substrate [8]–[10].

In the conventional CBD-CdS process, ammonia (NH_3) serves as the standard complexing agent. However, its high volatility causes progressive changes in bath pH, its toxicity poses environmental and occupational hazards, and its narrow effective process window reduces reproducibility under industrial conditions. Alternative complexing agents, including ethylenediaminetetraacetic acid (EDTA), triethanolamine (TEA), sodium citrate, glycine, and acetylacetone, have therefore been investigated as replacements or supplements [11]–[14].

Table 1: Some published reports on complexing agents in CdS depositions

	Complexing Agent(s)	Reported Structure	Novelty	Reference
1.	Standard ammonia bath (CBD)	Nanometric CdS layers	Established baseline nanolayer CBD process for device application	[16]
2.	Ammonia vs. EDTA	Ammonia -> hexagonal (rough); EDTA -> cubic, smoother	First direct demonstration that complexing agent choice dictates crystal phase and morphology	[10]
3.	EDTA-assisted	Hexagonal; improved crystallinity vs. ammonia-only	EDTA chelation slows deposition rate, yielding more compact films	[13]
4.	Selective/controlled chelation route	Crystalline nanospheres	Demonstrated high stability and optical uniformity of nanosphere CdS via tailored complexation	[12]
5.	Sodium citrate (ammonia-free)	Hexagonal	Ammonia-free process improved environmental /process safety; comparable optical quality.	[14]
6.	Varied complexing agents + deposition time	Hierarchical nanoflake structures	Showed that complexing agent identity directly controls crystallite size, phase, and morphology	[15]

CdS films prepared using EDTA exhibit a cubic crystal structure, in contrast to the hexagonal structure obtained with ammonia, which exhibits poor morphology and undesirable optical properties for solar cell applications [10]. Kumar et al. demonstrated that the choice of complexing agent directly influences crystallite size, crystal phase, and film morphology in CBD-CdS systems [15].

Despite this growing body of work (Table 1), an understanding of the structure–property–performance relationships arising from different chemistries of complexing and supplementary agents remains limited. This study investigates the use of acetylacetone as a supplementary co-complexing agent alongside ammonia, rather than as a sole or replacement complexing agent, on the structural, morphological, optical, and electrical properties of CBD-deposited CdS thin films, with direct implications for the performance of heterojunction solar cell's buffer layers.

2 Experimental Procedure

2.1 Substrate Preparation

Glass substrates were ultrasonically cleaned sequentially in acetone and absolute ethanol for 15 minutes each, followed by thorough rinsing with deionized water (resistivity ≥ 18.2 MΩ·cm). Cleaned substrates were dried under nitrogen and stored in a desiccator until use.

2.2 Chemical Bath Preparation and Deposition

CdS thin films were deposited by chemical bath deposition using cadmium acetate dihydrate [$Cd(CH_3CO_2)_2{\cdot}2H_2O$] and thiourea [$CH_4N_2S$] as the cadmium and sulfur precursor sources, respectively. Aqueous ammonia solution (NH_4OH) served as the primary complexing agent. The reagents were combined in a fixed molar ratio of Cd^{2+} : thiourea: NH_4OH = 1:1:2.5.

Table 2: Summary of CBD-CdS deposition parameters

Parameter	Sample I (with acetylacetone)	Sample II (without acetylacetone)
Cadmium source	$Cd(CH_3CO_2)_2{\cdot}2H_2O$	
Sulfur source	Thiourea (CH_4N_2S)	
Complexing agent(s)	NH_4OH + Acetylacetone (≥ 99%)	NH_4OH only
Molar ratio Cd:Th:NH_3	1: 1: 2.5	
Bath temperature	70 ± 3 °C	
Deposition time	20 minutes	
Bath volume	200 ml	
Stirring condition	300 rpm	
Substrate	Glass	

For Sample I (with acetylacetone), 0.04 mL of acetylacetone (purity ≥ 99%) was introduced into the bath as an auxiliary co-complexing agent. Sample II was prepared under identical conditions without acetylacetone (Table 2).

Substrates were immersed vertically in the chemical bath maintained at 70 ± 3 °C in a thermostatically controlled water bath. Depositions lasted 10 – 20 minutes. After deposition, the coated substrates were gently rinsed with deionized water and dried at room temperature.

2.3 Film Characterization

Structural properties were analyzed by X-ray diffraction (XRD) using Cu Kα radiation (λ = 1.5406 Å) over a 2θ range of 10 – 80°. Surface morphology was examined by scanning electron microscopy (SEM, TESCAN VEGA3) operated at 6.0 kV in secondary electron mode. Elemental composition was assessed by energy-dispersive X-ray spectroscopy (EDX) coupled to the SEM. Surface topography was characterized by atomic force microscopy (AFM) over a 2.0 × 2.0 μm² scan area using NT-MDT NTEGRA Spectra in semi-contact mode, with images obtained in ambient conditions and no special sample preparation, and analyzed using the IA-P9 software. Optical transmittance and absorbance spectra were recorded by a Jasco-V-670 spectrophotometer (300 – 900 nm), and optical bandgap energies were determined from Tauc plots of $(\alpha h\nu)^2$ vs. hν. Electrical transport properties were evaluated using Hall-effect measurements in the van der Pauw configuration. The film thickness, determined using a Bruker DektakXT® Stylus surface profilometer, was approximately 120 nm.

3 Results and Discussions

The use of acetylacetone to chelate Cd^{2+} ions reportedly lower the concentration of free metal ions in solution due to relative supersaturation, which depends on the difference between the actual concentration and the solubility limit, where the binding effectively reduces the thermodynamic driving force for rapid nucleation and crystal growth [17], [18].

By acting as a ligand, acetylacetone binds Cd^{2+}, effectively reducing the amount of "unbound" metal available to react with counterpart ions, i.e., S^{2-}, keeping the system below critical supersaturation thresholds [19]–[21]. The controlled release of cadmium and subsequent formation of CdS follow the thermodynamic balance, in Equations 1a-1c:

$$Cd^{2+} + 2acac^- \rightleftharpoons [Cd(acac)_2] \quad (1a)$$

$$(NH_2)_2CS + 2OH^- \rightleftharpoons CH_2N_2 + 2H_2O \quad (1b)$$

(1)

$$Cd^{2+}_{(released)} + S^{2-} \longrightarrow CdS_{(s)} \quad (1c)$$

The solubility product (K_{sp}) of CdS is very small. So even a tiny amount of free cadmium is enough to initiate growth, making the buffering effect of acetylacetone essential for a smooth reaction [17], [22], [23].

3.1 Structural Characterization

The XRD patterns of both samples (Figure 1) reveal diffraction peaks at 2θ ≈ 26.5°, 44.0°, and 51.8°, corresponding to the (002), (110), and (201) reflection planes of the hexagonal wurtzite phase of CdS (JCPDS Card No. 41-1049, space group $P6_3mc$).

Both films exhibit preferential orientation along (002), indicating c-axis growth perpendicular to the substrate surface, a texture associated with minimization of surface free energy during nucleation [24], [25]. No secondary phases (CdO, $Cd(OH)_2$) were detected, confirming phase purity.

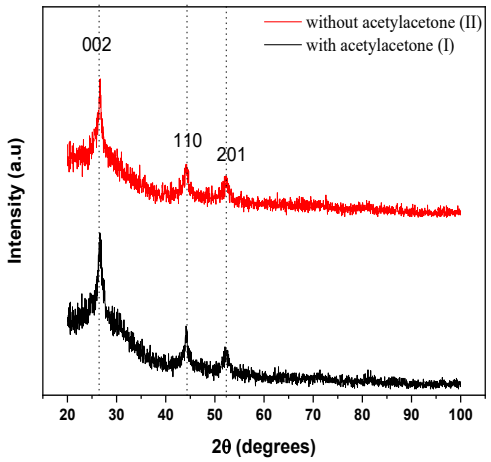

Figure 1: XRD patterns of both samples

Sample II (without acetylacetone) showed slightly lower diffraction peaks, indicating a more extensively crystallized film. Sample I (with acetylacetone) showed a dominant (002) peak with lesser and broadened (110) and (201) reflections, consistent with a lower supersaturation enforced by the Cd^{2+} chelation of acetylacetone [17], [18]. The crystallite size (D), dislocation density (δ), and micro strain (ε) were estimated from the (002) peak using the Equations 2-4 [26], [27]:

$$D = \frac{K\lambda}{\beta \cos\theta} \quad (2)$$

where K is the dimensionless shape factor (taken as 0.94 for spherical crystallites), λ is the X-ray wavelength (Cu Kα, λ = 1.5406 Å), β is the full width at half maximum (FWHM) of the diffraction peak in radians, and θ is the Bragg diffraction angle. The lower FWHM of the (002) peak in Sample I relative to that in Sample II suggests a larger average crystallite size in the acetylacetone-modified film, indicating that complexing agents in CBD lead to finer-grained, more uniform CdS films [10].

The dislocation density (δ), defined as the number of dislocation lines per unit volume of crystalline material, was estimated using:

$$\delta = \frac{1}{D^2} \quad (3)$$

Furthermore, the micro strain (ε) was evaluated from:

$$\varepsilon = \frac{\beta \cos\theta}{4} \quad (4)$$

The higher dislocation density and microstrain in Sample II (Table 3) are due to the smaller crystallite size and the lattice distortions introduced by the constrained growth environment. These structural defects, while potentially acting as recombination centers, may be partially mitigated by appropriate post-deposition annealing treatments, which have been reported to improve crystallinity and reduce defect density in CBD-CdS films [28].

The absence of detectable diffraction peaks attributable to CdO, $Cd(OH)_2$, or elemental sulfur in either diffractogram suggests high phase purity within the detection limits of XRD. It indicates that the reaction conditions, particularly the ammonia-to-cadmium ratio and a bath temperature of 70 ± 3 °C, were sufficient to ensure the selective deposition of CdS without significant formation of competing phases.

This is an important finding for buffer-layer applications, as the presence of secondary phases, such as $Cd(OH)_2$, at the CdS/absorber interface has been shown to introduce interface states that degrade open-circuit voltage and fill factor in CIGS solar cells [3].

Table 3: Structural parameters derived from XRD analysis

Parameter	Sample I (with acetylacetone)	Sample II (without acetylacetone)
Phase	Hexagonal wurtzite	Hexagonal wurtzite
Preferred orientation	(002)	(002)
Peaks observed	(002), (110), (201)	(002), (110), (201)
FWHM of (002) (°)	0.3936	0.6298
Crystallite size D (nm)	21.7	13.5
Dislocatidensity δ (x 10^{-4} nm^{-2})	21.3	54.6
Microstrain ε (x10^{-3})	7.25	11.6

Collectively, the XRD results demonstrate that both deposition routes yield phase-pure hexagonal CdS films with a preferential (002) orientation. At the same time, acetylacetone exerts a measurable influence on crystallinity, peak multiplicity, and crystallite size by modulating bath chemistry.

The quantitative structural parameters derived from these diffractograms are summarized in Table 3.

3.2 Morphological Characterization

The SEM micrograph (Figure 2, TESCAN VEGA3, 6.0 kV, 50,000×, view field 2.77 µm) reveals a film surface densely populated with well-defined, quasi-spherical nanoparticles uniformly distributed across the substrate.

The globular grain morphology with smooth, rounded boundaries is indicative of an ion-by-ion heterogeneous nucleation and growth mechanism characteristic of CBD under controlled supersaturation [14], [25]. Average grain sizes range from 50 to 100 nm, consistent with the nanocrystalline character inferred from XRD.

Dark contrast regions between grain clusters indicate intergranular voids and incomplete surface coalescence, attributable to the short deposition time window (10 – 20 min). Grain agglomerates with a diameter of 150 – 200 nm are also observed, consistent with Ostwald ripening at 70 °C [10].

The presence of acetylacetone is expected to moderate agglomeration through its sustained Cd^{2+} chelation, limiting the reactive ion supply available for rapid secondary grain growth. The 50 – 100 nm grain-size range is optimal for CdS buffer layers in CIGS and CdTe solar cells, maximizing the absorber contact area while limiting grain-boundary recombination [28].

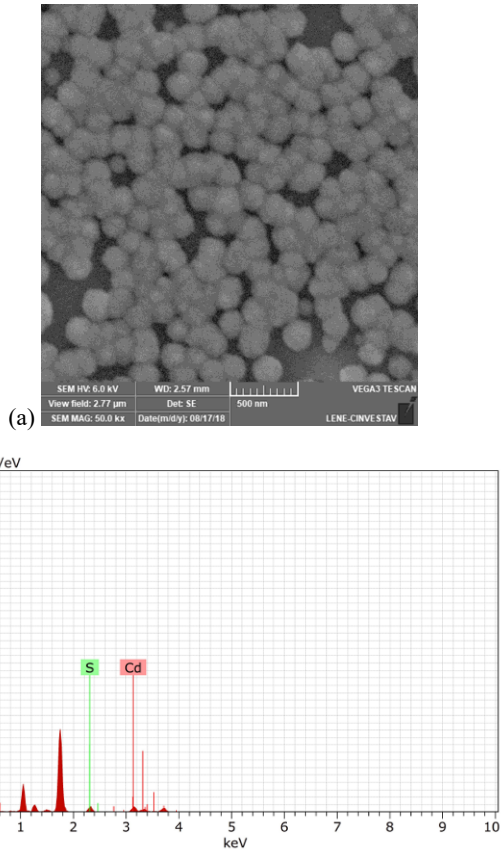

Figure 2: (a) SEM micrograph of the sample deposited with acetylacetone and (b) EDX spectrum of the sample deposited with acetylacetone

The EDX spectrum (Figure 2b) confirms binary CdS composition through characteristic emission lines. Emission signals attributable to oxygen, carbon, or any other impurity element were detected across the full 0 – 10 keV energy range. The absence of oxygen signals confirms that the competing phases (i.e., CdO and $Cd(OH)_2$) are below the EDX detection limit (~ 0.1 at.%), corroborating the XRD phase-purity result.

Also, the absence of carbon, despite the use of carbon-containing precursors (cadmium acetate, acetylacetone), confirms that the deposition conditions are sufficient to prevent the incorporation of organic residue [3].

3.3 Surface Topography

AFM topographic imaging over a 2.0 × 2.0 µm² scan area (Figure 3, scale bar 0.4 µm) reveals an anisotropic surface morphology dominated by elongated, ridge-like features oriented diagonally (~ 45° to the x-axis), with lateral dimensions of ~ 0.3 – 0.5 µm in width and ~ 0.8 – 1.2 µm in length, separated by inter-ridge valleys. The total peak-to-valley Z-height is ~ 27 nm, indicating a comparatively low overall surface relief. All parameters are documented in Table 4.

This elongated grain architecture reflects the lateral coalescence of primary nanoparticles into extended aggregates – a hierarchical assembly mechanism well documented in CBD chalcogenide films [28].

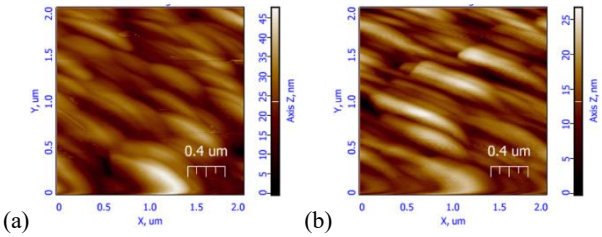

(a) (b)

Figure 3: Topography of the sample (a) with acetylacetone and (b) without acetylacetone

Table 4: AFM surface topographic parameters

Parameter	Sample I (with acetylacetone)	Sample II (without acetylacetone)
Scan area	2.0 × 2.0 µm²	
Z-axis (height) range	0 – ~27 nm	
Dominant feature morphology	Elongated ridges / coalesced grain agglomerates	
Measured size (nm)	199	157
Feature orientation	Diagonal (~45° to x-axis); anisotropic	
Estimated RMS roughness (Rq) (nm)	6.27	3.98
Skewness	0.203	0.135
Kurtosis	3.71	3.06
Peak-to-valley height	~ 27 nm	
Surface coverage	Continuous; no exposed substrate regions	

The directional anisotropy of the ridge features is consistent with the anisotropic growth kinetics of hexagonal wurtzite CdS: faster growth along the c-axis ([001] direction, associated with the dominant (002) XRD reflection) manifests as elongated grain morphologies in plan-view AFM imaging [14]. The estimated RMS roughness (Rq ~ 3 – 8 nm) falls well within the <10 nm threshold considered acceptable for conformal contact between the CdS buffer layer and absorber surfaces, ensuring uniform junction formation without shunting pathways [3].

3.4 Optical Characterization: Bandgap Analysis

The optical bandgap (E_g) was determined by the Tauc method for direct allowed transitions, plotting $(\alpha h\nu)^2$ against hν and extrapolating the linear absorption edge to $(\alpha h\nu)^2 = 0$, as shown in Equation 5:

$$(\alpha h\nu)^2 = A(h\nu - E_g) \quad (5)$$

The reported bandgaps of CdS materials, depending on their physical form and synthesis method, range from 2.0 eV to 3.5 eV [29], [30]. The estimated bandgaps for the samples (Figure 4) were 2.62 eV and 2.87 eV for samples deposited with and without acetylacetone, respectively. The lower bandgap estimated upon the addition of acetylacetone reflects good crystalline quality and chemical stoichiometry, attributable to the controlled nucleation environment provided by acetylacetone [10].

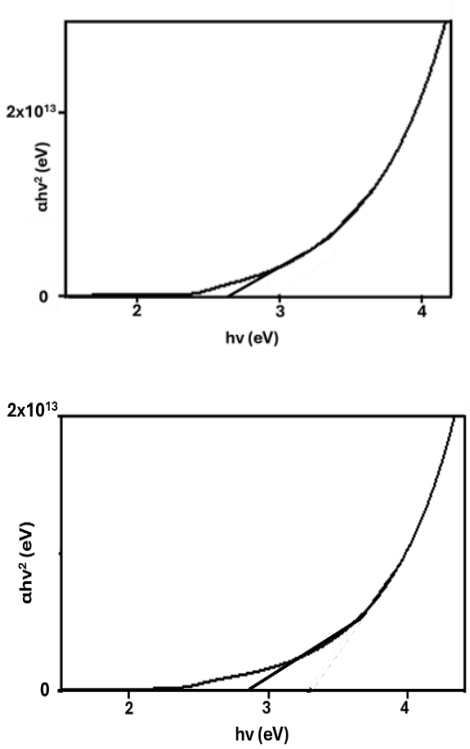

(a)

(b)

Figure 4: Estimated bandgaps of the sample (a) with acetylacetone and (b) without acetylacetone

3.5 Electrical Characterization

Considering the comparative properties of the sample deposited with acetylacetone, further characterization of its electrical properties was carried out (Table 5). The Hall coefficient (R_H) of the sample was estimated at -1.55 × 10^8 cm³/C. The negative sign unambiguously confirms n-type

electrical conductivity, consistent with the expected behavior of CBD-grown CdS, where sulfur vacancies and cadmium interstitials act as shallow donors [28]. The large absolute magnitude of R_H directly reflects the very low free-electron concentration through the relation $R_H = -1/(ne)$. The calculated free electron concentration, $n = 4.02 \times 10^{10}$ cm^{-3}, is very low, at the lower end of the range reported for CBD-CdS films ($10^{10} – 10^{17}$ cm^{-3}).

This is directly attributable to the near-stoichiometric Cd:S incorporation promoted by acetylacetone chelation, which reduces the sulfur vacancy and cadmium interstitial concentrations relative to the ammonia-only process. The low carrier concentration implies a long Debye screening length and a wide space-charge region at the heterojunction, both of which are favorable for high V_{oc} in completed solar cell devices [3].

The Hall mobility of μ_H, estimated at 49.2 cm^2/V·s, places the sample at the upper end of reported values for CBD-CdS films (typically 5 – 50 cm^2/V·s), reflecting high crystalline quality with efficient electron transport [28]. The elevated mobility is consistent with the larger grain dimensions and the lower grain boundary density inferred from SEM and XRD analyses, as grain boundaries are primary sites of momentum relaxation in polycrystalline CdS. The reduced ionized impurity scattering associated with the low carrier concentration further enhances mobility [31]. Internal consistency of the Hall data is confirmed by the relation (Equation 6).

$$\begin{aligned} \sigma &= ne\mu_H \\ &= (4.02 \times 10^{10})(1.602 \times 10^{-19})(49.2) \\ &\approx 3.16 \times 10^{-7}\ (\Omega\cdot cm)^{-1} \end{aligned} \quad (6)$$

which is consistent with the measured $\rho = 3.78 \times 10^6\ \Omega\cdot$cm.

Table 5: Summarized Hall effect electrical parameters for the measured sample I

Parameter	Sample I (with acetylacetone)
Hall coefficient R_H (cm^3/C)	-1.55×10^8
Carrier type	n-type
Carrier concentration n (cm^{-3})	4.02×10^{10}
Hall mobility μ_H (cm^2/V·s)	49.2
Resistivity ρ (Ω·cm)	3.78×10^6
Optical bandgap E_g (eV)	~ 2.42
Dominant scattering	Grain boundary (low ionized impurity)
Buffer layer suitability	Excellent

The electrical resistivity ($\rho = 3.78 \times 10^6\ \Omega\cdot$cm) indicates that the sample is a high-resistivity semiconductor approaching semi-insulating behavior. This high resistivity, a direct consequence of the very low carrier concentration, reduces parasitic shunt leakage and improves V_{oc} by maintaining a high potential barrier at the heterojunction. For ultrathin CdS buffer layers (50 – 80 nm) in high-efficiency CIGS and CdTe devices, the series-resistance contribution remains manageable. The improved interface quality of low-defect-density, high-resistivity films generally outweighs the series-resistance penalty [28].

Conclusion

This study presents a comprehensive investigation into the effects of acetylacetone, an auxiliary co-complexing agent, on the properties of CBD-deposited CdS thin films for solar cell buffer-layer applications. XRD confirmed the hexagonal wurtzite phase in both samples with (002) preferred orientation and phase purity. SEM revealed quasi-spherical nanoparticles of 50 – 100 nm, and EDX confirmed exclusive binary CdS composition free of organic or oxide contamination. AFM revealed a smooth, anisotropic surface topography with peak-to-valley heights of ~27 nm, consistent with conformal heterojunction formation. Optical bandgap analysis yielded a near-ideal $E_g \sim 2.42$ eV for Sample I vs. a blue-shifted ~ 2.55–2.60 eV for Sample II, attributed to a higher donor defect density and Burstein-Moss band filling in the ammonia-only film.

This study successfully demonstrated that using acetylacetone as a supplementary co-complexing agent alongside ammonia, rather than as a sole or replacement complexing agent, as reported in previous studies with EDTA, TEA, citrate, or glycine systems, helped to achieve, for the first time, a CBD-CdS buffer layer with a near-ideal stoichiometric bandgap (~ 2.42 eV) combined with an exceptionally low carrier concentration (4.02×10^{10} cm^{-3}), high Hall mobility (49.2 cm^2/V·s), and high resistivity ($3.78 \times 10^6\ \Omega\cdot$cm), thereby establishing, through a unified structural–morphological–optical–electrical correlation, that controlled bidentate Cd^{2+} chelation can simultaneously suppress defect-related band filling and produce a low-defect, near-stoichiometric film suited to high-efficiency heterojunction solar cells while reducing reliance on ammonia.

Further studies will focus on optimizing the acetylacetone concentration and integrating the optimized CdS buffer into complete CIGS or CdTe solar cell devices.

Acknowledgments

The author appreciates fellow colleagues for their support and assistance.

Credit author statement

Onyekachi Nwakanma: Conceptualization, Investigation, Writing-Original draft, Reviewing and Editing**.**

Declaration of Competing Interest

The author discloses no personal or financial conflicts that might have affected the research.

References

[1] M. A. Green et al., "Solar Cell Efficiency Tables (Version 66)," Prog. Photovoltaics Res. Appl., vol. 33, no. 7, pp. 795–810, Jul. 2025, doi: 10.1002/pip.3919.

[2] J. Cheng et al., "High-efficiency Sb2Se3 thin-film solar cells based on Cd(S,O) buffer layers prepared via spin-coating," Mater. Chem. Phys., vol. 303, p. 127794, Jul. 2023, doi: 10.1016/j.matchemphys.2023.127794.

[3] S. Sinha, D. K. Nandi, P. S. Pawar, S.-H. Kim, and J. Heo, "A review on atomic layer deposited buffer layers for Cu(In,Ga)Se2 (CIGS) thin film solar cells: Past, present, and future," Sol. Energy, vol. 209, pp. 515–537, Oct. 2020, doi: 10.1016/j.solener.2020.09.022.

[4] D. A. Garzón et al., "Zn 1− x Sn x O y Buffer Layer Deposited by Chemical Bath Deposition for Low and Wide Bandgap Cu(In, Ga)Se 2 Solar Cells," Adv. Energy Sustain. Res., vol. 7, no. 1, Jan. 2026, doi: 10.1002/aesr.202500307.

[5] I. M. Beker, F. B. Dejene, L. F. Koao, J. J. Terblans, S. Z. Werta, and A. U. Yimamu, "Influence of Electrolytic Bath pH on the Structural, Morphological, and Optical Properties of CdTe:Se Thin Films Prepared by Electrodeposition for Solar Cell Application," J. Electron. Mater., vol. 54, no. 8, pp. 6575–6585, Aug. 2025, doi: 10.1007/s11664-025-12082-4.

[6] A. U. Yimamu, S. Z. Werta, F. T. Maremi, B. F. Dejene, and O. K. Echendu, "Effect of deposition voltage on the physico-chemical properties of electrodeposited Mg-doped CdS thin films for Opto-electronic application," Mater. Today Commun., vol. 42, p. 111410, Jan. 2025, doi: 10.1016/j.mtcomm.2024.111410.

[7] C. Kamal et al., "Enhanced photovoltaic performance of Cu-doped CdS quantum dots for solar cell applications: a deposition using SILAR technique," J. Mater. Sci. Mater. Electron., vol. 36, no. 20, p. 1281, Jul. 2025, doi: 10.1007/s10854-025-15352-3.

[8] T. Nasrin et al., "Exploring ionic liquid assisted chemical bath deposition of a highly uniform and transparent cadmium sulfide thin film for photovoltaic applications," RSC Adv., vol. 15, no. 7, pp. 4892–4903, 2025, doi: 10.1039/D4RA06320A.

[9] V. Ramya, K. Neyvasagam, R. Chandramohan, S. Valanarasu, and A. M. F. Benial, "Studies on chemical bath deposited CuO thin films for solar cells application," J. Mater. Sci. Mater. Electron., vol. 26, no. 11, pp. 8489–8496, Nov. 2015, doi: 10.1007/s10854-015-3520-3.

[10] H. Zhang, X. Ma, and D. Yang, "Effects of complexing agent on CdS thin films prepared by chemical bath deposition," Mater. Lett., vol. 58, no. 1–2, pp. 5–9, Jan. 2004, doi: 10.1016/S0167-577X(03)00394-X.

[11] M. C. Acosta-Enriquez et al., "Nanometric layers of Cadmium Sulphide by CBD and a potential application," WSEAS Trans. Circuits Syst., vol. 9, no. 3, pp. 133–142, Mar. 2010, doi: 10.5555/1852275.1852276.

[12] A. L. Leal-Cruz et al., "Microstructural and optical characterizations of highly stable nanospheres of crystalline CdS via selective approach," Opt. Mater. Express, vol. 4, no. 1, p. 129, Jan. 2014, doi: 10.1364/OME.4.000129.

[13] W. G. C. Kumarage et al., "Growth and characterization of EDTA assisted CBD-CdS," Mater. Chem. Phys., vol. 200, pp. 1–8, Oct. 2017, doi: 10.1016/j.matchemphys.2017.07.052.

[14] R. Ochoa-Landín, J. Sastre-Hernández, O. Vigil-Galan, and R. Ramírez-Bon, "Chemically deposited CdS by an ammonia-free process for solar cells window layers," Sol. Energy, vol. 84, no. 2, pp. 208–214, Feb. 2010, doi: 10.1016/j.solener.2009.11.001.

[15] A. Kumar, D. Pednekar, S. Mukherjee, and R. K. Choubey, "Effect of deposition time and complexing agents on hierarchical nanoflake-structured CdS thin films," J. Mater. Sci. Mater. Electron., vol. 31, no. 19, pp. 17055–17066, Oct. 2020, doi: 10.1007/s10854-020-04263-0.

[16] M. Kokotov, Y. Feldman, A. Avishai, M. DeGuire, and G. Hodes, "Chemical bath deposition of CdS highly-textured, columnar films," Thin Solid Films, vol. 519, no. 19, pp. 6388–6393, Jul. 2011, doi: 10.1016/j.tsf.2011.04.096.

[17] Y. Xu et al., "High quality CdS buffer layer developed via Zn salt additive engineering for Sb 2 S 3 solar cells," New J. Chem., vol. 49, no. 15, pp. 6143–6150, 2025, doi: 10.1039/D4NJ05036C.

[18] S. Ningev and J. Gbertyo, "Chelation Effect of 2 , 4-Pentadione with Ni (II) and Cu (II) Ions," vol. 6, no. 2, pp. 48–57, 2021.

[19] R. M. Kellogg and M. Leeman, "9.16 Crystallization as a Tool in Industrial Applications of Asymmetric Synthesis," in Comprehensive Chirality, Elsevier, 2012, pp. 367–399.

[20] A. Hussein, "Principles of Flow Assurance Solids Formation Mechanisms," in Essentials of Flow Assurance Solids in Oil and Gas Operations, Elsevier, 2023, pp. 143–197.

[21] C. van der Geest, A. Melchuna, L. Bizarre, A. C. Bannwart, and V. C. B. Guersoni, "Critical review on wax deposition in single-phase flow," Fuel, vol. 293, p. 120358, Jun. 2021, doi: 10.1016/j.fuel.2021.120358.

[22] E. D. Spoerke et al., "Nanocrystal Layer Deposition: Surface-Mediated Templating of Cadmium Sulfide Nanocrystals on Zinc Oxide Architectures," J. Phys. Chem. C, vol. 113, no. 37, pp. 16329–16336, Sep. 2009, doi: 10.1021/jp900564r.

[23] I. S. Akinsola, A. B. Alabi, A. A. Ajayi, K. S. Adedayo, and O. A. Babalola, "Effect of substrate temperature on optical properties of spray pyrolytic cadmium sulphide thin films," Jordan J. Phys., vol. 12, no. 3, pp. 191–200, 2019.

[24] C. Körber, J. Suffner, and A. Klein, "Surface energy controlled preferential orientation of thin films," J. Phys. D. Appl. Phys., vol. 43, no. 5, p. 055301, Feb. 2010, doi: 10.1088/0022-3727/43/5/055301.

[25] G. Carter, "Preferred orientation in thin film growth — the survival of the fastest model," Vacuum, vol. 56, no. 2, pp. 87–93, Feb. 2000, doi: 10.1016/S0042-207X(99)00171-2.

[26] A. Morán, O. Nwakanma, S. Velumani, and H. Castaneda, "Comparative study of optimised molybdenum back-contact deposition with different barriers (Ti, ZnO) on stainless steel substrate for flexible solar cell application," J. Mater. Sci. Mater. Electron., vol. 31, no. 10, pp. 7524–7538, May 2020, doi: 10.1007/s10854-020-03058-7.

[27] O. Nwakanma, P. Reyes, and S. Velumani, "Electrical, structural, and topographical properties of direct current (DC) sputtered bilayer molybdenum thin films," J. Mater. Sci. Mater. Electron., vol. 29, no. 18, pp. 15671–15681, Sep. 2018, doi: 10.1007/s10854-018-9165-2.

[28] A. Ashok, G. Regmi, A. Romero-Núñez, M. Solis-López, S. Velumani, and H. Castaneda, "Comparative studies of CdS thin films by chemical bath deposition techniques as a buffer layer for solar cell applications," J. Mater. Sci. Mater. Electron., vol. 31, no. 10, pp. 7499–7518, May 2020, doi: 10.1007/s10854-020-03024-3.

[29] W. Ismail, G. Ibrahim, M. A. Habib, O. K. Alduaij, M. Abdelfatah, and A. El-Shaer, "Advancement of Physical and Photoelectrochemical Properties of Nanostructured CdS Thin Films toward Optoelectronic Applications," Nanomaterials, vol. 13, no. 11, p. 1764, May 2023, doi: 10.3390/nano13111764.

[30] H. Moualkia, S. Hariech, and M. S. Aida, "Structural and optical properties of CdS thin films grown by chemical bath deposition," Thin Solid Films, vol. 518, no. 4, pp. 1259–1262, Dec. 2009, doi: 10.1016/j.tsf.2009.04.067.

[31] B. G. Streetman and S. Banerjee, Solid state electronic devices, Sixth. Prentice Hall New Jersey, 2005.